

# Influence of Pulse Parameters on the Morphology and Corrosion Resistance of Nickel-Graphene Composite Coating

Xin Yu, Ruiyu Zhang, Gan Cui, Zili Li\*

China University of Petroleum (East China), College of Pipeline and Civil Engineering, Qingdao 266580, China

\*E-mail: [zilimenhuzu@163.com](mailto:zilimenhuzu@163.com)

*Received:* 7 January 2019 / *Accepted:* 23 February 2019 / *Published:* 10 April 2019

---

Ni-graphene composite coatings were electrodeposited on mild steel substrate in Watt plating solution containing suspended graphene oxide (GO). Raman spectra confirmed the reduction of GO during the deposition process. Furthermore, effects of graphene concentration and electrodeposition parameters including current density, pulse frequency, and duty cycle were investigated by electrochemical tests and various characterization techniques. Morphology and anti-corrosion properties of the Ni-graphene coatings electrodeposited under different parameters were evaluated by scanning electron microscopy, potentiodynamic polarization, and electrochemical impedance spectroscopy. The results showed that the Ni-graphene composite coating, deposited at the GO concentration of 0.2 g·L<sup>-1</sup>, current density of 6 A·dm<sup>-2</sup>, frequency of 50 Hz, and duty cycle of 0.4, exhibited uniform morphology and dense structure. The corrosion current density of Ni-graphene coating prepared under optimal parameters is an order of magnitude smaller than that of pure Ni coating.

---

**Keywords:** nickel-graphene, composite coating, electrodeposition parameter, corrosion resistance

## 1. INTRODUCTION

Nickel (Ni) and its alloy have attracted significant attention considering their favorable corrosion resistance and toughness [1]. Ni deposits improve the appearance, extend the life and performance of different materials, and they have potential industrial applications. Extensive research efforts have been devoted to investigate the reinforced Ni matrix with various strengthening particles, such as tungsten carbide [2, 3], alumina [4, 5], carbon nanotube [6, 7], and diamond [8, 9]. The main objective of synthesizing composite coatings is to enhance the properties that can hardly be achieved using pure Ni coatings. Electrodeposition is one of the most effective methods to develop composites because of a better control over structures through regulations of pulse parameters.

Graphene is strictly a two-dimensional material that exhibits mechanical stiffness, inertia, and impermeability [10], which is beneficial for enhancing the performance of anticorrosion coatings. Recently, several studies employed graphene as reinforcement in composite coatings.

Kuang et al. [11] first synthesized Ni-based graphene coating by electrodeposition, which exhibited improved thermal conductivity and hardness. Kumar et al. [12] prepared Ni-graphene coatings from the plating bath containing reduced graphene oxide (rGO,  $100 \text{ mg}\cdot\text{L}^{-1}$ ). The Ni-graphene coatings showed higher corrosion resistance compared to the pure Ni coating. Xue et al. [13] studied the influence of duty cycle on the mechanical properties and microstructure of Ni-GO composite coatings electrodeposited under supercritical carbon dioxide. The composite coating showed the highest micro-hardness and the best wear resistance when deposited at the duty cycle of 0.25. Jabbar et al. [14] investigated the effects of deposition temperature on the surface morphology and corrosion resistance of electrodeposited Ni-graphene composite coatings.

In this study, Ni-graphene composite coatings were deposited on mild steel by pulse electrodeposition. The effects of GO concentration, deposition current density, frequency and duty cycle on the surface morphology and corrosion behavior of coatings were studied.

## 2. EXPERIMENTAL

### 2.1 Preparation of graphene oxide

GO was prepared from graphite flakes ( $\leq 30 \text{ }\mu\text{m}$ , CP grade) by the modified Hummer's method [15]. The chemicals used in the preparation process are listed in Table 1, and the reagents were not further purified before use.

**Table 1.** Chemical reagents used for experiments.

Reagent	$\text{NaNO}_3$	$\text{H}_2\text{SO}_4$	$\text{KMnO}_4$	$\text{H}_2\text{O}_2$	HCl
property	99.0%, AR	98.0%, GR	99.5%, AR	30.0%, AR	36.0%~38.0%, AR

Briefly, concentrated sulfuric acid (250 mL) was taken in a dry beaker, and the beaker was placed in an ice-water bath (below  $10 \text{ }^\circ\text{C}$ ) and subjected to magnetic stirring. Then the mixture of graphite powder (5 g) and sodium nitrate (4 g) was added into the beaker containing acid. Potassium permanganate powder (25 g) was slowly added for about 1 h and this low temperature reaction stage lasted for 2 h. The beaker was then transferred to a  $35 \text{ }^\circ\text{C}$  oil bath and the contents were stirred for 2 h, followed by the addition of deionized water. After maintaining the temperature at  $95 \text{ }^\circ\text{C}$  for 40 min, ice cubes prepared using deionized water were added to bring the temperature of solution down to room temperature. Hydrogen peroxide solution was added until no bubble generated and the color of the solution turned bright yellow. Then the suspension was centrifuged and rinsed first by dilute hydrochloric acid ( $1 \text{ mol}\cdot\text{L}^{-1}$ ) and then by deionized water to remove the residual salts and acids until the pH of the graphene dispersion was close to 7. The solution was diluted to 500 mL and was further exfoliated in a 300 W ultrasonic water bath, while the temperature was kept below  $45 \text{ }^\circ\text{C}$ .

## 2.2 Electrodeposition

The substrate material under study was mild steel with a size of 30 mm×20 mm×2 mm, and its chemical composition is listed in Table 2. To ensure the flatness and neatness of the sample to be plated, the substrate was gradually polished using water abrasive paper until 2000 grade.

The surfaces of the sample were insulated, except the working area to be plated. Before electrodeposition, the sample was alkali-washed at 75 °C for 10 min, and the composition of the alkali wash is summarized in Table 3. Further, the sample was pickled in hydrochloric acid (10 wt.%) to remove oxides and activate the sample, thereby enhancing the bonding force between the deposits and substrate.

**Table 2.** Chemical composition of 20 # steel (wt.%).

Element	C	Si	Mn	P	S	Ni	Cr	Cu
wt.%	0.190	0.280	0.520	0.035	0.035	0.030	0.025	0.025

**Table 3.** Chemical composition of alkali wash lotion.

Component	NaOH	Na <sub>2</sub> CO <sub>3</sub>	Na <sub>2</sub> SiO <sub>3</sub> ·9H <sub>2</sub> O
Concentration (g/L)	12	60	30

The composition of the plating bath is listed in Table 4. The GO suspension was added to a certain concentration according to the experimental parameters, and the pH of the solution was adjusted to 3.6±0.1 using dilute sulfuric acid and aqueous ammonia. The pretreated sample was attached to the cathode of a plating power source (Dashun, SMD-P), and a Ni plate (99.5% purity) as anode was placed 6 cm away opposite the cathode. The electrodeposition was carried out in a water bath maintained at 50 °C, with magnetic stirring at 200 r·min<sup>-1</sup> for 30 min.

**Table 4.** Chemical composition of plating bath.

Component	NiSO <sub>4</sub> ·6H <sub>2</sub> O	NiCl <sub>2</sub> ·6H <sub>2</sub> O	H <sub>3</sub> BO <sub>3</sub>	C <sub>12</sub> H <sub>25</sub> NaO <sub>4</sub> S
Concentration (g/L)	280.0	40.0	35.0	0.5

## 2.3 Analysis and characterization

Atomic force microscopy (AFM, Brooke, Multimode) was used to test the morphology and thickness of graphene sheets. Scanning electron microscopy (SEM, FEI Company's Nova Nano SEM450) with spectral scanning function was used to investigate the surface morphology and elemental content. Raman spectroscopy (THERMO, DXR-type) was utilized to characterize GO and composite coating.

Electrochemical impedance spectroscopy (EIS) was carried out using the PARSTAT 2273 electrochemical workstation and to obtain the potentiodynamic polarization curve of coating. The entire electrochemical test process used a standard three-electrode system. The working electrode was

encapsulated specimen with exposed test area of  $1 \text{ cm}^2$ , the auxiliary electrode was a platinum electrode, and the reference electrode was a saturated calomel electrode. The experiments were carried out at room temperature and the corrosive medium was 3.5 wt.% NaCl solution. The EIS test was performed after the system was stabilized, when the change of open circuit potential (OCP) was below  $\pm 3 \text{ mV}$  within 300 s specifically. The EIS was carried out at a frequency range of 10 mHz~100 kHz with 10 mV AC potential signal varied from open potential. The potentiodynamic polarization scanning was carried out within the range of  $\pm 25 \text{ mV}$  for various OCP values at the scan rate of  $0.5 \text{ mV} \cdot \text{s}^{-1}$ .

### 3. RESULTS AND DISCUSSION

#### 3.1 Characterization of Graphene oxide

Fig. 1 shows the AFM image and the thickness variation of the Z-height profile of as-prepared GO sheets. Measurement of the thickness of multiple samples revealed that the thickness distribution of GO was in the range of 2–5 nm, indicating that the GO sheet existed as a single layer or few layers graphene (no more than seven layers) in solution [16].

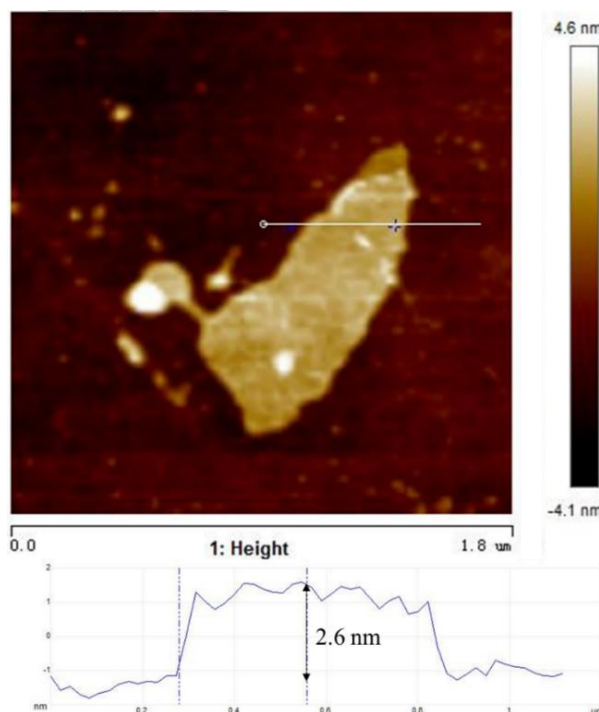


**Figure 1.** Tapping mode AFM image and cross-section analysis of  $12 \text{ ng} \cdot \mu\text{L}^{-1}$  GO dispersion.

#### 3.2. Surface characterization

Fig. 2 exhibits the SEM images showing wrinkled-like flakes partly embedded in Ni matrix on the coating surface. To determine the existence of graphene, energy-dispersive X-ray spectroscopy (EDS) element mapping was tested at area observed on flake structure. The X-ray energy spectra of the target

area are shown in Fig. 3. The high carbon content (56.4 wt.%) preliminarily confirmed the incorporation and well dispersion of graphene.

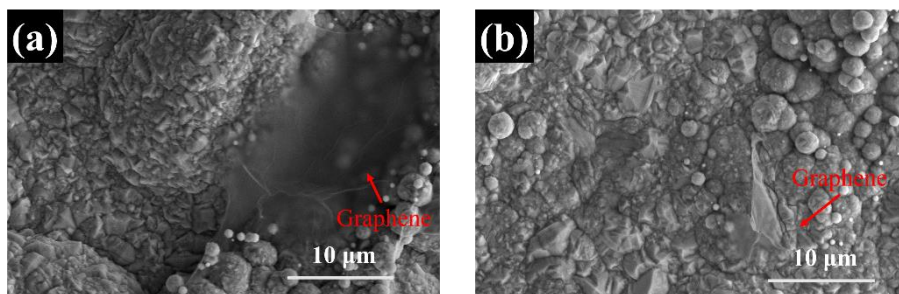


Figure 2. SEM images of graphene sheets on composite coatings.

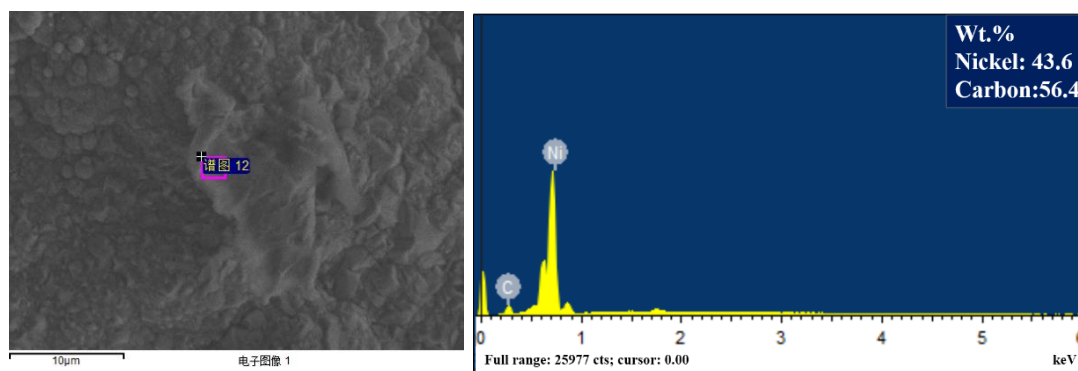


Figure 3. EDS mapping of the area observed on graphene on composite coating.

The Raman spectra of freeze-dried GO, pure Ni coating and Ni-graphene composite coating are shown in Fig. 4. Raman spectra of pure Ni coatings do not show the appearance of any peak, while the Raman spectra of GO and Ni-graphene composite coatings exhibit similar pattern, indicating successful incorporation of graphene.

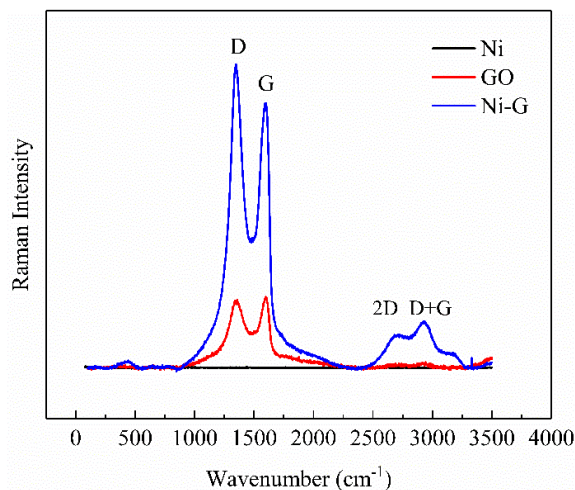
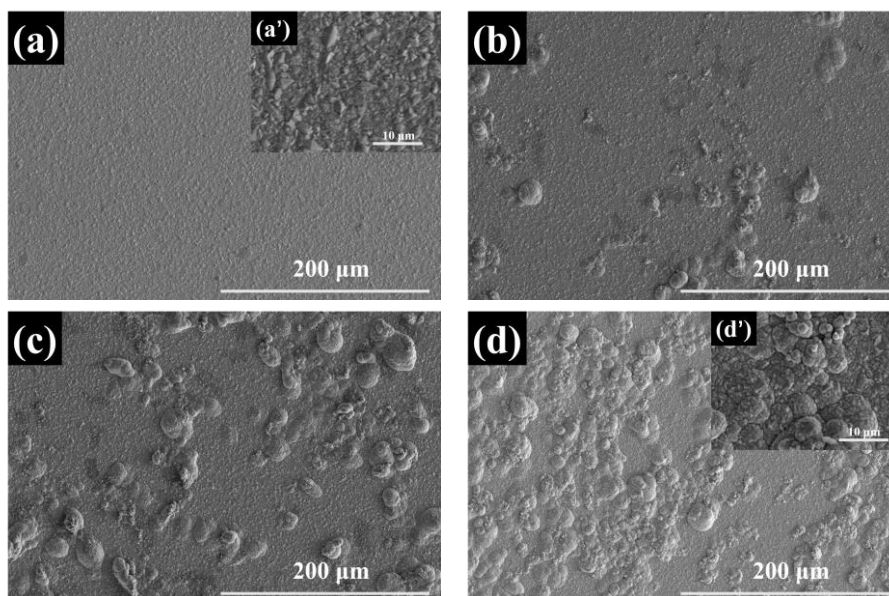


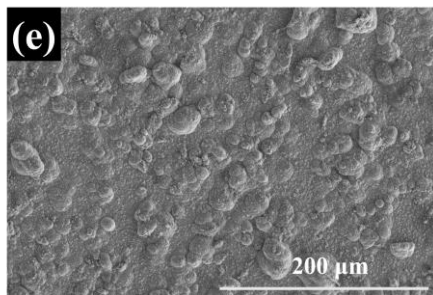
Figure 4. Raman spectra of pristine GO, Ni coating and Ni-graphene composite coating.

The main features in the Raman spectra of graphitic carbon-based materials are the G and D peaks and their overtones. The Raman spectrum of GO displays two strong peaks at  $1350\text{ cm}^{-1}$  (D band) and  $1600\text{ cm}^{-1}$  (G band) and two weak peaks at  $2690\text{ cm}^{-1}$  (2D band) and  $2940\text{ cm}^{-1}$  (D+G band). The intensity ratio of D band and G band ( $I_D/I_G$ ) can characterize the disorder of graphene [17, 18]. The D/G intensity ratio of GO is 0.957, while the intensity ratio of Ni-graphene composite coating shifts to 1.147, indicating the reduction of GO [19]. Moreover, the intensity of 2D band and D+G band of Ni-graphene coating increased after deposition compared to that of GO, which indicates the presence of bulk rGO and the formation of defects during the reduction [20, 21].

### 3.3 Effects of deposition parameters on the surface morphology of coatings

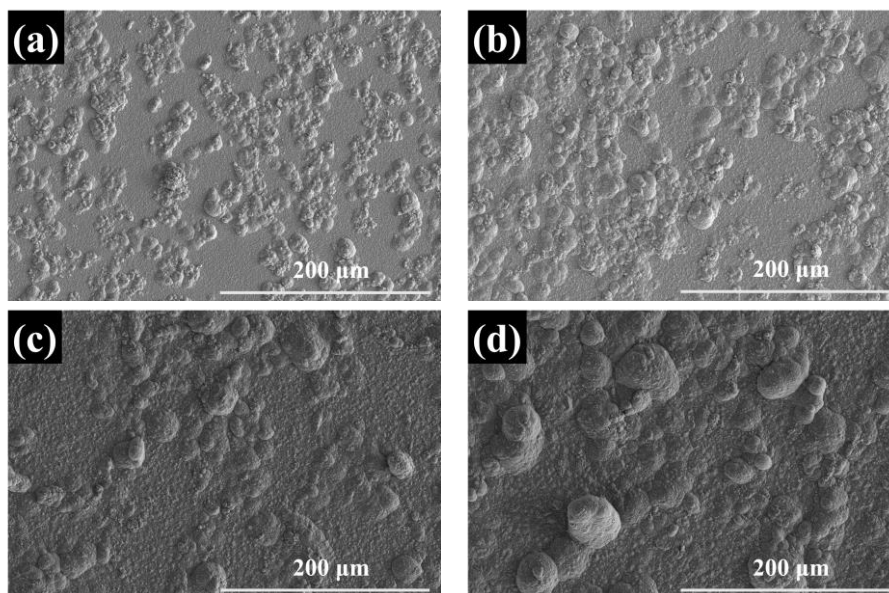
The SEM images of coatings deposited from the bath with different GO concentrations are illustrated in Fig. 5. Morphology of pure Ni coating (Fig. 5(a)) is characterized by the dense structure and uniform grain size [11], and the rhombic grain with hard edges is observed at the magnification of 10000 (Fig. 5(a')). With the incorporation of graphene flakes, the surface roughness of coatings increased [21] and nodular structures appeared. When the concentration of GO was low ( $0.05$  or  $0.1\text{ g}\cdot\text{L}^{-1}$ ), the coating surface was incompletely covered with graphene. When the plating bath contained  $0.2\text{ g}\cdot\text{L}^{-1}$  GO (Fig. 5(d)), the nodular features uniformly appeared on coating surface. The spherical growth of composite coating was observed under higher magnification (Fig. 5(d')), which was first demonstrated by Yasin et al. [20]. The spheres-like morphology led to the improvement in the micro-hardness and corrosion resistance of Ni-graphene nanocomposite coatings. However, when the concentration of GO reached  $0.3\text{ g}\cdot\text{L}^{-1}$ , many bulges were observed, possibly caused by the restacking and agglomeration of GO flakes. Thus GO concentration of  $0.2\text{ g}\cdot\text{L}^{-1}$  was considered as the optimal value for obtaining uniform coating surface with spherical structural morphology.

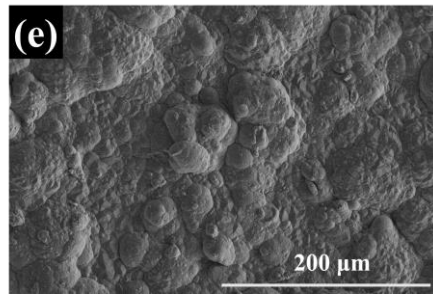




**Figure 5.** SEM micrographs of (a) pure Ni coating; and Ni-graphene composite coating obtained at GO concentration of (b)  $0.05 \text{ g}\cdot\text{L}^{-1}$ , (c)  $0.1 \text{ g}\cdot\text{L}^{-1}$ , (d)  $0.2 \text{ g}\cdot\text{L}^{-1}$ , and (e)  $0.3 \text{ g}\cdot\text{L}^{-1}$ .

The morphologies of Ni-graphene composite coatings prepared at different deposition current densities are illustrated in Fig. 6. When the current density is low, the cathode shows limited adsorption capacity for metal cations and GO flakes. The characteristic nodular features appear incompletely on the surface of the coating (Fig. 6(a)). With the increase in the current density to  $6 \text{ A}\cdot\text{dm}^{-2}$ , the nucleation rate of Ni and content of graphene increase. This leads to the inhibition of nucleus growth and optimization of grain structure [22]. When the current density exceeds  $6 \text{ A}\cdot\text{dm}^{-2}$ , the peak current density is much higher than the average current density. Once the pulse electrical signal was turned on, the metal cations near the cathode were rapidly reduced, causing grain coarsening and protrusions formation (Figs. 6(d, and e)). At the same time, the hydrogen evolution reaction on cathode surface was exacerbated, thus causing stress accumulation and defects such as pinholes and microcracks. As a result, current density of  $6 \text{ A}\cdot\text{dm}^{-2}$  was considered as the optimized value.

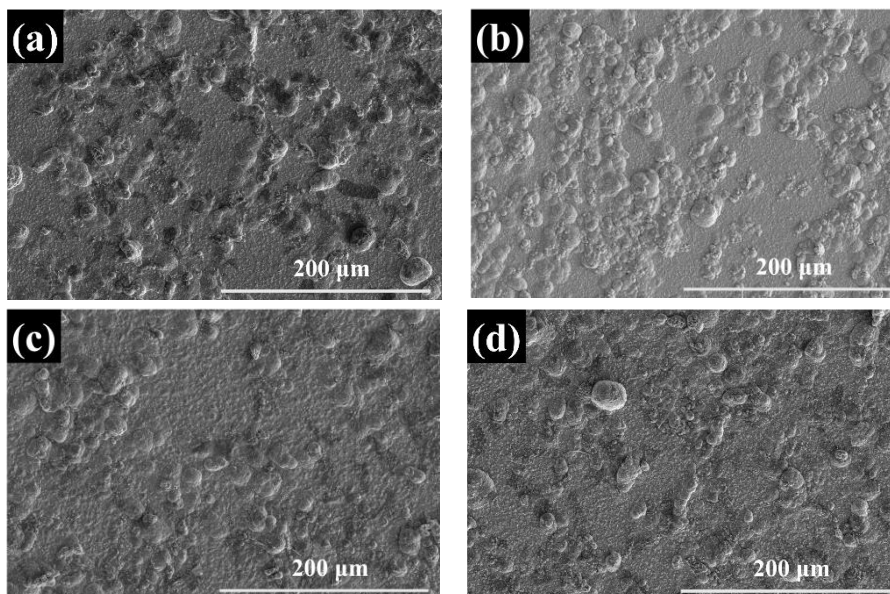




**Figure 6.** SEM micrographs of Ni-graphene composite coating obtained at current density of (a) 3 A·dm<sup>-2</sup>, (b) 6 A·dm<sup>-2</sup>, (c) 9 A·dm<sup>-2</sup>, (d) 12 A·dm<sup>-2</sup>, and (e) 15 A·dm<sup>-2</sup>.

The SEM images of Ni-graphene composite coatings deposited at different frequencies (32, 50, 100, 200 and 400 Hz) are shown in Fig. 7. When the deposition frequency is 32 Hz, the time of pulse period is relatively long and the concentration polarization near the electrode is severe. The dispersion of Ni<sup>2+</sup> and GO flakes fails to overcome the limitation of diffusion layer during the turn-off period.

The coating deposited at the frequency of 50 Hz exhibits even grain structure (Fig. 7(b)). However, when the frequency is further increased (100 Hz and above), the single pulse period is too short, and the electric double layer cannot be fully charged and discharged due to the capacitance effects [23]. Once the charging and discharging time is longer than turn-on and turn-off time, the pulse electrodeposition signal gradually shifts to direct current and loses the benefits of pulse plating. Moreover, the cathode surface concentration polarization is severe, thus the number of protrusions increases and the surface flatness decreases. Thus, pulse frequency of 50 Hz was selected as the optimized value for obtaining uniform morphology and dense structure of composite coating.



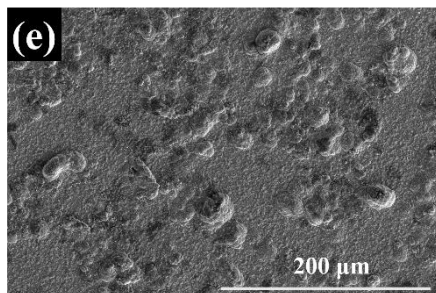


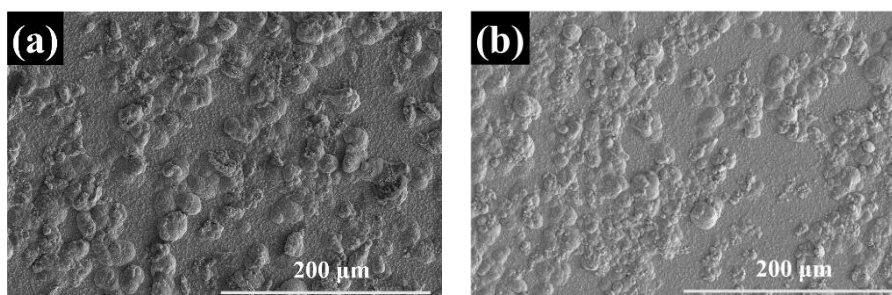
**Figure 7.** SEM micrographs of Ni-graphene composite coating obtained at frequency of (a) 32 Hz, (b) 50 Hz, (c) 100 Hz, (d) 200 Hz, and 400 Hz (e).

The SEM images of Ni-graphene composite coatings deposited at different duty cycles are shown in Fig. 8. Obviously, with the increase of duty cycle, the density of nodular features appearing on coating surface decreases (Figs. 8(a-e)), thus indicating the decrease of graphene content.

The thickness of the diffusion layer was found dependent on diffusion coefficient ( $D$ ) of metal ions and the turn-on time according to the equation shown below [24]:

$$\delta_p = \left( \frac{D_0 t_{on}}{\pi} \right)^{\frac{1}{2}} \quad (1)$$

With the extension of turn-on time, the thickness of diffusion layer increases. Under the condition of DC electrodeposition (duty cycle: 1), the conduction time is the total time of electrodeposition, and the grains keep on coarsening along the preferred orientation. The periodic turn-off of pulse electrical signals is beneficial to the precipitation of microbubbles and the restructuring of grain structure. When the duty ratio is 0.8 or 0.6, the on-time is long, and the diffusion speed of graphene flakes is inferior to that of the reduction of  $\text{Ni}^{2+}$ . According to literature [25, 26], the graphene sheets are more likely to enter the electric double layer and embed into the metal matrix with the extension of turn-off time. The graphene flakes also served as growth points for  $\text{Ni}^{2+}$  that could promote nucleation and inhibit grain growth. Fig. 8(b) shows the coating deposited at 0.4 duty cycle with refined crystal grains and improved crystal compactness. However, when the duty ratio is 0.2, the average current density is much smaller than peak current density and the nucleation speed is much larger than the crystal growth rate, which may cause the lattice distortion. Thus, duty cycle of 0.4 was selected as the optimized value.



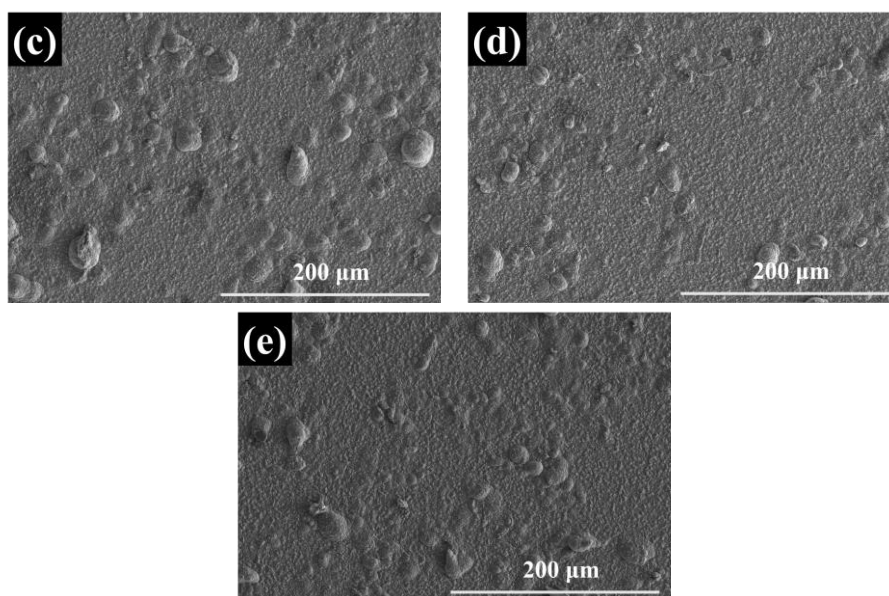


**Figure 8.** SEM micrographs of Ni-graphene composite coatings obtained at duty cycle of (a) 0.2, (b) 0.4, (c) 0.6, (d) 0.8, and (e) 1.

### 3.4 Corrosion behavior

The polarization curves and extrapolation fitting results of the coatings prepared at different graphene contents in depositing bath are shown in Fig. 9 and Table 5.

The pure Ni coating showed low corrosion potential and the highest corrosion current density, indicating higher corrosion tendency for pure Ni coating. The improvement in corrosion resistance of the Ni-graphene composite coating was attributed to the impermeability of graphene which could effectively prevent the penetration of corrosive media [27]. Moreover, the graphene sheet distributed on the surface of the coating could reduce the active surface area of sample, which could reduce the ion transfer rate and inhibit the diffusion behavior of corrosive  $\text{Cl}^-$ . The corrosion potential of the composite coating reached the highest value when the GO concentration was  $0.2 \text{ g}\cdot\text{L}^{-1}$ , and the corrosion current density decreased to  $2.24 \times 10^{-8} \text{ A}\cdot\text{cm}^{-2}$ , which was an order of magnitude lower than that of pure Ni coating ( $1.30 \times 10^{-7} \text{ A}\cdot\text{cm}^{-2}$ ). Furthermore, the corrosion resistance of deposited composite coating in 3.5 wt.% NaCl solution was preferable than that of Ni-graphene composite coatings on carbon steel ( $i_{\text{corr}} = 2.766 \times 10^{-7} \text{ A}\cdot\text{cm}^{-2}$ ,  $E_{\text{corr}} = -0.119$ ) prepared by Jabbar et al. [14]. However, agglomeration was likely to occur between the GO flakes during the co-deposition process when the GO concentration was at or above  $0.2 \text{ g}\cdot\text{L}^{-1}$ . The degradation of flatness and compactness eventually led to the decrease of corrosion resistance. Rekha et al. [28] reported that the corrosion rate of SnNi-graphene composite coatings progressively decreased with the increase of GO content. However, the effect of pulse electrodeposition parameters on properties of the coating was not always reported the same, but there existed optimal electrodeposition parameters.

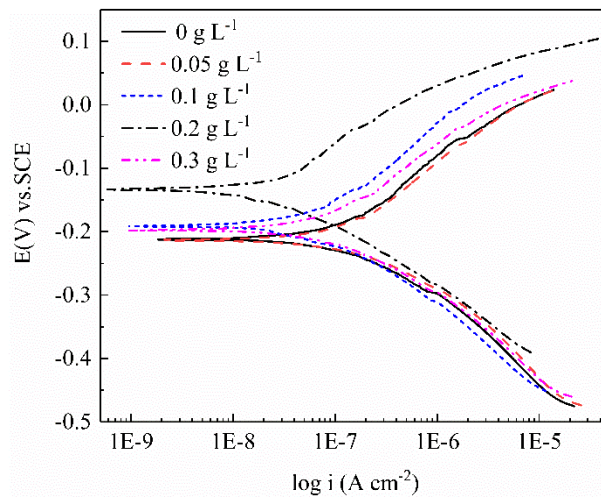


**Figure 9.** Potentiodynamic polarization curves of coatings obtained at GO concentrations of 0, 0.05, 0.1, 0.2, and 0.3 g·L<sup>-1</sup> at a scan rate of 0.5 mV·s<sup>-1</sup> in 3.5 wt.% NaCl solution.

**Table 5.** Corrosion parameters determined from the potentiodynamic polarization plots for Ni-G coatings deposited at different GO concentrations.

GO concentration (g·L <sup>-1</sup> )	$E_{corr}$ (mV)	$i_{corr}$ (A·cm <sup>-2</sup> )	$\beta_c$ (mV)	$\beta_a$ (mV)
0.00	-211	$1.3 \times 10^{-7}$	100	147
0.05	-210	$1.4 \times 10^{-7}$	110	129
0.10	-191	$7.0 \times 10^{-8}$	104	138
0.20	-131	$2.2 \times 10^{-8}$	93	101
0.30	-195	$9.5 \times 10^{-8}$	106	126

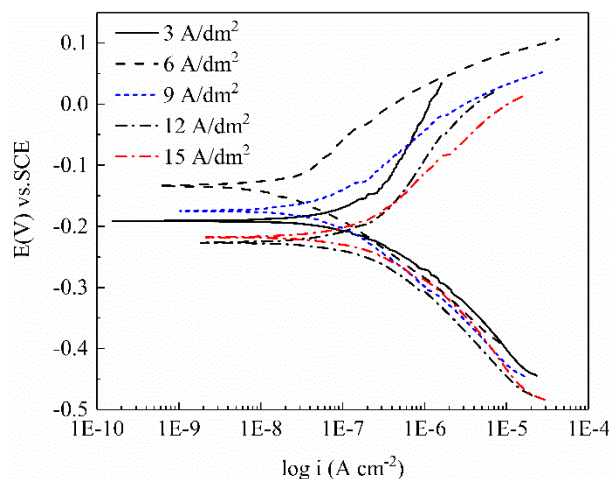


**Figure 10.** Potentiodynamic polarization curves of coatings obtained at current densities of 3, 6, 9, 12, and 15 A·dm<sup>-2</sup> at a scan rate of 0.5 mV·s<sup>-1</sup> in 3.5 wt.% NaCl solution.

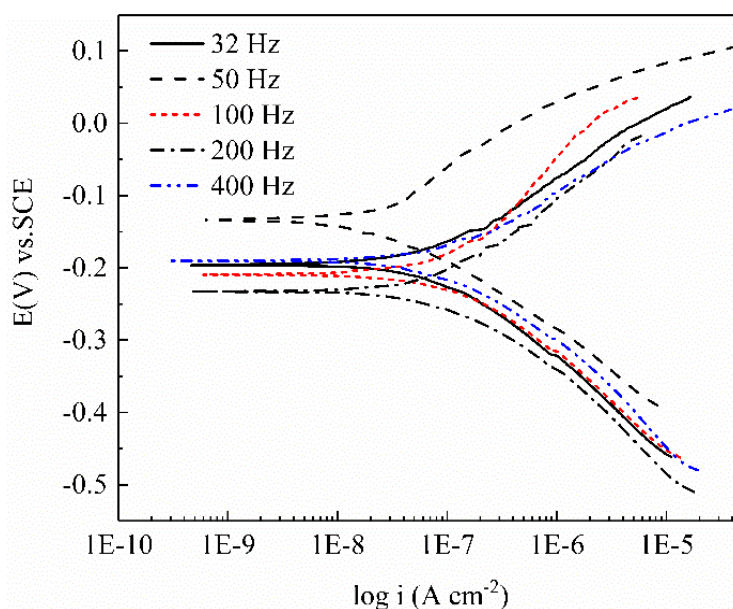
Fig. 10 and Table 6 show the comparative analysis of the polarization curves and kinetic parameters of the Ni-graphene coatings under different electrodeposited current densities, indicating that with the increased deposition current density the corrosion current density decreased until it reached the minimum value ( $2.24 \times 10^{-8}$  A·dm<sup>-2</sup>). The corrosion potential acquired the most positive value at the

optimal deposition current density of  $6 \text{ A}\cdot\text{dm}^{-2}$ . The Ni-graphene coatings deposited at optimal deposition current density of  $6 \text{ A}\cdot\text{dm}^{-2}$  have preferable corrosion resistance.

**Table 6.** Corrosion parameters determined from the potentiodynamic polarization plots for Ni-G coatings deposited at different current densities.

Current density ( $\text{A}\cdot\text{dm}^{-2}$ )	$E_{\text{corr}}$ (V)	$i_{\text{corr}}$ ( $\text{A}\cdot\text{cm}^{-2}$ )	$\beta_{\text{c}}$ (mV)	$\beta_{\text{a}}$ (mV)
3	-190	$2.4\times 10^{-7}$	127	273
6	-131	$2.2\times 10^{-8}$	93	101
9	-170	$7.3\times 10^{-8}$	109	111
12	-225	$2.3\times 10^{-7}$	132	204
15	-215	$2.0\times 10^{-7}$	118	129

Fig. 11 shows the polarization plots of the coatings prepared under different pulse frequencies. When the pulse frequency is 50 Hz, the self-corrosion potential of the samples is the most positive and the corrosion tendency is the least. The fitted kinetic parameters of each sample in 3.5 wt.% NaCl solution are listed in Table 7. With the increase in the pulse frequency, the corrosion current density of the coating decreases until it reaches minimum value ( $2.24 \times 10^{-8} \text{ A}\cdot\text{cm}^{-2}$ ) at 50 Hz. At this time, the self-corrosion potential was the highest, indicating that the corrosion resistance of the prepared coating at 50 Hz was the best. Further increase in the deposition frequency would lead to increasing grain boundary [29], thus leading to the decline of anti-corrosion performance.

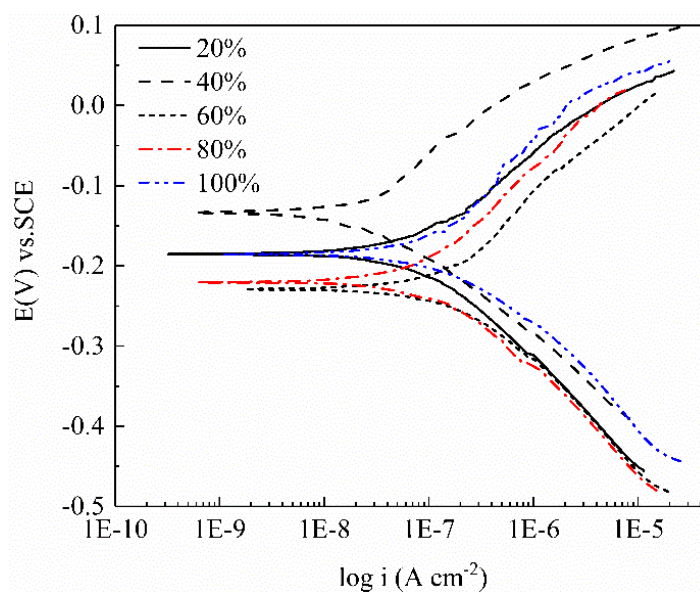


**Figure 11.** Potentiodynamic polarization curves of coatings obtained at frequencies of 32, 50, 100, 200, and 400 Hz at a scan rate of  $0.5 \text{ mV}\cdot\text{s}^{-1}$  in 3.5 wt.% NaCl solution.

**Table 7.** Corrosion parameters determined from the potentiodynamic polarization plots for Ni- graphene coatings deposited at different frequencies.

Frequency (Hz)	$E_{\text{corr}}$ (V)	$i_{\text{corr}}$ ( $\text{A}\cdot\text{cm}^{-2}$ )	$\beta_{\text{c}}$ (mV)	$\beta_{\text{a}}$ (mV)
32	-193	$7.9\times 10^{-8}$	123	104
50	-131	$2.2\times 10^{-8}$	93	101
100	-207	$1.3\times 10^{-7}$	128	169
200	-229	$9.2\times 10^{-8}$	119	113
400	-189	$10.0\times 10^{-8}$	123	89

Fig. 12 and Table 8 represent the polarization curves of the coating under different duty cycles and the corrosion kinetic parameters obtained by fitting. When the duty ratio is 0.4, the self-corrosion current density reaches the minimum value and the self-corrosion potential is the most positive, indicating that the corrosion resistance of the coating layer is optimal under this condition. Xue et. al. also reported the benefit of the existence of off-time to grain refinement and the existence of optimal duty cycle [13].

**Figure 12.** Potentiodynamic polarization curves of coatings obtained at duty cycles of 0.2, 0.4, 0.6, 0.8, and 1 at a scan rate of  $0.5 \text{ mV}\cdot\text{s}^{-1}$  in 3.5 wt.% NaCl solution.**Table 8.** Corrosion parameters determined from the potentiodynamic polarization plots for Ni- graphene coatings deposited at different duty cycles.

Duty cycle (%)	$E_{\text{corr}}$ (V)	$i_{\text{corr}}$ ( $\text{A}\cdot\text{cm}^{-2}$ )	$\beta_{\text{c}}$ (mV)	$\beta_{\text{a}}$ (mV)
20	-182	$7.3\times 10^{-8}$	121	102
40	-131	$2.2\times 10^{-8}$	93	101
60	-227	$1.6\times 10^{-7}$	122	134
80	-218	$1.1\times 10^{-8}$	114	158
100	-183	$1.2\times 10^{-8}$	108	144

#### 4. CONCLUSIONS

In this study, nickel (Ni) -graphene composite coatings were synthesized on mild steel by pulse electrodeposition. The graphene flakes partly embedded in Ni matrix were observed on the coating surface by SEM, and the reduction of GO was confirmed by Raman spectroscopy. The effect of graphene concentration, deposition current density, pulse frequency, and duty cycle was studied in detail by electrochemical test and SEM observation. The Ni-graphene composite coatings prepared at the optimal process parameters of  $0.2 \text{ g}\cdot\text{L}^{-1}$  graphene oxide,  $6 \text{ A}\cdot\text{dm}^{-2}$  deposition current density, 50 Hz frequency, and 0.4 duty cycle provided uniform and dense structure as well as the most satisfying corrosion resistance in 3.5 wt.% NaCl solution.

#### References

1. J. Xu, J. Tao, S. Jiang, Z. Xu, *Appl Surf Sci.*, 254 (2008) 4036.
2. N. Elkhoshkhany, A. Hafnway, A. Khaled, *J Alloys Compd.*, 695 (2017) 1505.
3. S. Mohajeri, A. Dolati, S. Rezagholibeiki, *Mater Chem Phys.*, 129 (2011) 746.
4. Z. Shafiee, M.E. Bahrololoom, B. Hashemi, *Mater Design.*, 108 (2016) 19.
5. S.W. Jiang, L. Yang, J.N. Pang, H. Lin, Z.Q. Wang, *Surf Coat Tech.*, 286 (2016) 197.
6. G. Barati Darband, M. Aliofkhaezai, A. Sabour Rouhaghdam, *J Electroanal Chem.*, 829 (2018) 194.
7. C. Guo, Y. Zuo, X. Zhao, J. Zhao, J. Xiong, *Surf Coat Tech.*, 202 (2008) 3246.
8. H. Zhou, N. Du, L. Zhu, J. Shang, Z. Qian, X. Shen, *Electrochim Acta.*, 151 (2015) 157.
9. M. Sajjadnejad, H. Omidvar, M. Javanbakht, A. Mozafari, *J Alloys Compd.*, 704 (2017) 809.
10. A.K. Geim, K.S. Novoselov, *Nat Mater.*, 6 (2007) 183.
11. D. Kuang, L. Xu, L. Liu, W. Hu, Y. Wu, *Appl Surf Sci.*, 273 (2013) 484.
12. C.M.P. Kumar, T.V. Venkatesha, R. Shabadi, *Mater Res Bull.*, 48 (2013) 1477.
13. Z. Xue, W. Lei, Y. Wang, H. Qian, Q. Li, *Surf Coat Tech.*, 325 (2017) 417.
14. A. Jabbar, G. Yasin, W.Q. Khan, M.Y. Anwar, R.M. Korai, M.N. Nizam, G. Muhyodin, *RSC Adv.*, 7 (2017) 31100.
15. W.S. Hummers, R.E. Offeman, *J Am Chem Soc.*, 80 (1958) 1339.
16. J. Hou, C. Bao, S. Qu, X. Hu, S. Nair, Y. Chen, *Appl Surf Sci.*, 459 (2018) 185.
17. P. Ramesh, S. Bhagyalakshmi, S. Sampath, *J Colloid Interf Sci.*, 274 (2004) 95.
18. A.C. Ferrari, J. Robertson, *Phys Rev B.*, 61 (2000) 14095.
19. M. Hilder, B. Winther-Jensen, D. Li, M. Forsyth, D.R. MacFarlane, *Phys Chem Chem Phys.*, 13 (2011) 9187.
20. G. Yasin, M.A. Khan, M. Arif, M. Shakeel, T.M. Hassan, W.Q. Khan, R.M. Korai, Z. Abbas, Y. Zuo, *J Alloys Compd.*, 755 (2018) 79.
21. D. Cao, H. Li, Z. Wang, J. Wei, J. Wang, Q. Liu, *Synthesis, Thin Solid Films*, 597 (2015) 1.
22. Y. Xuetao, W. Yu, S. Dongbai, Y. Hongying, *Surf Coat Tech.*, 202 (2008) 1895.
23. S.A. Lajevardi, T. Shahrabi, J.A. Szpunar, *Appl Surf Sci.*, 279 (2013) 180.
24. D. Landolt, A. Marlot, *Surf Coat Tech.*, 169-170 (2003) 8.
25. S.A. Lajevardi, T. Shahrabi, *Appl Surf Sci.*, 256 (2010) 6775.
26. T. Nickchi, M. Ghorbani, *Surf Coat Tech.*, 203 (2009) 3037.
27. V. Berry, *Carbon*, 62 (2013) 1.

28. M.Y. Rekha, A. Kamboj, C. Srivastava, *Thin Solid Films*, 653 (2018) 82.
29. M.H. Allahyarzadeh, M. Aliofkhazraei, A.R.S. Rouhaghdam, V. Torabinejad, *J Alloys Compd.*, 666 (2016) 217.

© 2019 The Authors. Published by ESG ([www.electrochemsci.org](http://www.electrochemsci.org)). This article is an open access article distributed under the terms and conditions of the Creative Commons Attribution license (<http://creativecommons.org/licenses/by/4.0/>).